Boltzmann entropy of a freely expanding quantum ideal gas

Saurav Pandey[1], Junaid Majeed Bhat[1], Abhishek Dhar[1], Sheldon Goldstein[2], David A. Huse[3], Manas Kulkarni[1], Anupam Kundu[1] and Joel L. Lebowitz[2]

March 23, 2023

Abstract We study the time evolution of the Boltzmann entropy of a microstate during the non-equilibrium free expansion of a one-dimensional quantum ideal gas. This quantum Boltzmann entropy, S_B, essentially counts the "number" of independent wavefunctions (microstates) giving rise to a specified macrostate. It generally depends on the choice of macrovariables, such as the type and amount of coarse-graining, specifying a *non*-equilibrium macrostate of the system, but its extensive part agrees with the thermodynamic entropy in thermal equilibrium macrostates. We examine two choices of macrovariables: the U-macrovariables are local observables in position space, while the f-macrovariables also include structure in momentum space. For the quantum gas, we use a non-classical choice of the f-macrovariables. For both choices, the corresponding entropies s_B^f and s_B^U grow and eventually saturate. As in the classical case, the growth rate of s_B^f depends on the momentum coarse-graining scale. If the gas is initially at equilibrium and is then released to expand to occupy twice the initial volume, the per-particle increase in the entropy for the f-macrostate, Δs_B^f, satisfies $\log 2 \leq \Delta s_B^f \leq 2\log 2$ for fermions, and $0 \leq \Delta s_B^f \leq \log 2$ for bosons. For the same initial conditions, the change in the entropy Δs_B^U for the U-macrostate is greater than Δs_B^f when the gas is in the quantum regime where the final stationary state is not at thermal equilibrium.

Contents

[1] International Centre for Theoretical Sciences, Tata Institute of Fundamental Research, Bangalore 560089, India
[2] Departments of Mathematics and Physics, Rutgers University, Piscataway, NJ 08854, USA
[3] Physics Department, Princeton University, Princeton, NJ, 08544, USA

1 Introduction

Understanding the emergence of the second law for macroscopic systems from the reversible microscopic dynamics was the remarkable achievement of Boltzmann [1,2,3,4,5,6,7,8,9]. He constructed an entropy function, satisfying the second law, for a typical individual microstate X of a macroscopic system that is in a macrostate specified by the values of a collection of macrovariables. This Boltzmann entropy is defined for systems both in and out of equilibrium as the logarithm of the "number" of microstates corresponding to the system's macrostate. For a classical system, the microstates are specified by points X in phase space, and the Boltzmann entropy of X is, up to an additive constant, the logarithm of the phase space volume of the set of all microstates for which the macrovariables have the same values as they do for X. For a quantum system, the microstates are specified by wave functions $|\Phi\rangle$. This difference, which allows observables to have indeterminate values in the quantum microstate, can make the precise definition of quantum macrovariables and macrostates somewhat subtle [10,11,12,13], and also allows for new non-classical choices of macrovariables, as we illustrate below. The Boltzmann entropy of $|\Phi\rangle$ is then the logarithm of the number of independent wave functions that have the same values of the chosen macrovariables as $|\Phi\rangle$ does. At thermal equilibrium, for all proper choices of macrovariables this definition coincides, in its extensive part, with the thermodynamic entropy of Clausius [14].

In a previous paper some of the authors investigated the time evolution of the Boltzmann entropy for a freely expanding *classical* ideal gas, using two different choices of macrovariables [15]. In the present paper, we extend this to a freely expanding *quantum* ideal gas. We provide numerical results for the evolution of the microstates and the associated entropy functions during free expansion. We consider both fermions and bosons and present results in the low and high-temperature regimes.

Before moving on, we mention some of the earlier works relevant to our study. Quantum quench of non-interacting fermions under various protocols have been studied using Wigner functions in [16,17]. Lattice fermions evolving from domain wall initial conditions have been studied with a focus on the evolution of the density profile and the growth of entanglement entropy [18,19]. The diagonal entropy for isolated quantum systems has been studied [20] for both integrable and non-integrable cases. Some other recent relevant discussions of entropy in quantum systems in the nonequilibrium setting can be found in Refs. [21,22,23].

The rest of the paper is organized as follows. In Sec. (2) we discuss ideas related to the definition of macrovariables, macrostates and the Boltzmann entropy in quantum systems. In Sec. (3) we introduce the specific example that we will be analyzing in the paper. In Sec. (4) we define our model of a quantum ideal gas and discuss aspects of its microscopic evolution. In particular, we discuss properties of the single-particle density matrix in Sec. (4.1) and the Wigner distribution function in Sec. (4.2). In Sec. (5.1) we discuss the U-macrovariables and the corresponding Boltzmann entropy S_B^U. In Sec. (5.2) we define the single-particle basis of

states that are localized both in position and momentum space. This is then used to define the f-macrovariables and the Boltzmann entropy S_B^f for the quantum gas. In Sec. (6), we present the numerical results. The results for fermions are presented in Sec. (6.1) and for bosons in Sec. (6.2). We discuss and summarize our findings in Sec. (7).

2 Boltzmann entropy for quantum systems

We now discuss the construction of macrostates and the Boltzmann entropy for isolated macroscopic quantum systems. For a more detailed discussion see Refs. [10,11,12]. Consider a quantum system with a Hilbert space $\mathscr{H}$, whose wave function lies in an energy shell $\mathscr{H}_E$ of width $\Delta E \ll E$. As macro observables, one option is to choose a set of commuting coarse-grained operators $\{\hat{M}_k\}$, $k = 1, \ldots, J$, meaning that the eigenvalues of each operator are grouped into "bins" and all eigenvalues of that operator within each bin are set equal. The simultaneous diagonalization of all the $\hat{M}_k$ operators then provides a decomposition of the accessible Hilbert space into a sum of orthogonal subspaces $\mathscr{H}_\nu$,

$$\mathscr{H}_E = \bigoplus_\nu \mathscr{H}_\nu, \tag{1}$$

where $\nu = (\nu_1, \ldots, \nu_J)$ defines a macrostate, and $\mathscr{H}_\nu$ is the joint eigenspace of the $\hat{M}_k$ with eigenvalues ν_k. The $\mathscr{H}_\nu$ will be referred to as macro-spaces, with $|\mathscr{H}_\nu| = \dim \mathscr{H}_\nu$ the dimension of the corresponding macro-space. One then associates a Boltzmann entropy $S_\nu = k_B \ln |\mathscr{H}_\nu|$ to each of the macro-spaces. Let us denote by $\hat{P}_\nu$ the projector onto the space $\mathscr{H}_\nu$. Any microstate, which is a pure state $|\Phi\rangle$, is said to be in the macrostate ν if $|\Phi\rangle$ is almost in $\mathscr{H}_\nu$, i.e. if $\langle\Phi|\hat{P}_\nu|\Phi\rangle \approx 1$, and then its Boltzmann entropy is given by $S_B(|\Phi\rangle) = S_\nu$. It is expected for many systems, including the one we study here, that for appropriate physical macrovariables if the initial pure state $|\Phi(0)\rangle$ is in a given macrostate, the time-evolved microstate $|\Phi(t)\rangle$ will continue to be (at almost all times) in one single macrostate, i.e. Schrodinger cat-like states will not occur. The exception being when the system crosses from one macrostate to another.

As in the classical case, for a physical choice of the macrovariables, a particular macro-space has by far the largest dimension, which we refer to as the equilibrium macro-space and denote it by $\mathscr{H}_{\mathrm{eq}}$. It is characterized by the fact $|\mathscr{H}_{\mathrm{eq}}| = (1 - \epsilon)|\mathscr{H}_E|$, $\epsilon \ll 1$, which we take as a physical requirement for any proper choice of the macrovariables. We also say that a system is in equilibrium when its microstate $|\Phi\rangle$ is in, or almost in, $\mathscr{H}_{\mathrm{eq}}$.

Now consider the unitary time-evolution of a system that is initially prepared in a non-equilibrium pure quantum state $|\Phi(0)\rangle$. Non-equilibrium means that $|\Phi(0)\rangle$ is not in, or not almost in, the space $\mathscr{H}_{\mathrm{eq}}$. It starts in one of the other macro-spaces $\mathscr{H}_{\nu \neq \mathrm{eq}}$ and with time it moves between different macro-spaces until it eventually ends up in the equilibrium macro-space and stays there for almost all subsequent times. It is expected that the non-equilibrium system should evolve to macro-spaces of higher dimensions, leading to a monotonic growth of entropy. This is what we would like to demonstrate in an explicit example. It is important to note that we are able to define this Boltzmann entropy for the pure quantum state, $|\Phi(t)\rangle$, at any time [9].

Computing the Boltzmann entropy: We note that the entropy S_ν of the macrostate ν, and thus $S_B(|\Phi(t)\rangle)$ for $|\Phi(t)\rangle$ in $\mathscr{H}_\nu$, is equal to the Gibbs-von Neumann entropy of a

generalized microcanonical ensemble, which is a mixed state that is uniform over (the unit sphere of) $\mathscr{H}_\nu$. It is important to stress, however, that this generalized microcanonical ensemble is not what we take as an accurate microscopic description of the microstate; it is only being used as a construction to compute the Boltzmann entropy of the microstate $|\Phi(t)\rangle$ at time t. The Boltzmann entropy at a later time $t' > t$ is dictated by what macrostate the unitarily time-evolved microstate $|\Phi(t')\rangle$ at that time corresponds to. If we were to instead unitarily time-evolve the density matrix of this out-of-equilibrium generalized microcanonical ensemble, its Gibbs-von Neumann entropy would not change in contrast to the second law of thermodynamics. A typical out-of-equilibrium microstate will, as time advances, typically move to other macrostates of higher Boltzmann entropy, so the Boltzmann entropy thereby does obey the second law for almost all microstates. The macrostate does not time-evolve unitarily, due to it being constructed via a coarse-graining with suitably chosen macrovariables.

This generalized microcanonical ensemble that is used to calculate the Boltzmann entropy of the macrostate at time t may be replaced by an equilibrium ensemble for a fictitious system where constraints have been imposed on all macrovariables to have particular values ν. Then, since that is a macroscopic equilibrium system, the extensive part of its microcanonical entropy should be equal to the extensive part of the Gibbs-von Neumann entropy of an equivalent generalized canonical ensemble. This shows that we can arrive at a correct (to leading order) count of the number of independent microstates in $\mathscr{H}_\nu$ by calculating the Gibbs-von Neumann entropy of an equivalent generalized canonical ensemble. This is convenient because in many cases, calculating properties is simpler in the canonical ensemble than in the microcanonical ensemble.

If we accept, as is argued above, that the Boltzmann entropy of the microstate $|\Phi(t)\rangle$ of a macroscopic system is equal, to leading order in system size, to the Gibbs-von Neumann entropy of a properly chosen generalized canonical ensemble, this allows us to skip the step of defining the generalized microcanonical ensemble. We use the expectation values, $\langle \hat{M}_k \rangle = \langle \Phi(t)|\hat{M}_k|\Phi(t)\rangle$, $k = 1, \ldots J$, to define the "equivalent" generalized canonical (GC) ensemble as

$$\hat{\rho}_{\mathrm{GC}} = \frac{e^{-\sum_k \lambda_k \hat{M}_k}}{Z_{\mathrm{GC}}}, \tag{2}$$

$$\text{where} \quad Z_{\mathrm{GC}} = \mathrm{Tr}\Big[e^{-\sum_k \lambda_k \hat{M}_k}\Big], \tag{3}$$

and the Lagrange multipliers λ_k are obtained from the constraint equations

$$Tr[\hat{M}_k \hat{\rho}_{\mathrm{GC}}] = \langle \hat{M}_k \rangle, \ k = 1, \ldots, J. \tag{4}$$

The resulting Boltzmann entropy S_B for the microstate $|\Phi(t)\rangle$ and the choice of $\{\hat{M}_k\}$ is then given by

$$S_B = k_B \sum_k \lambda_k \langle \hat{M}_k \rangle + k_B \ln Z_{\mathrm{GC}}. \tag{5}$$

We note that this is also equal to the maximum value of the Gibbs-von Neumann entropy

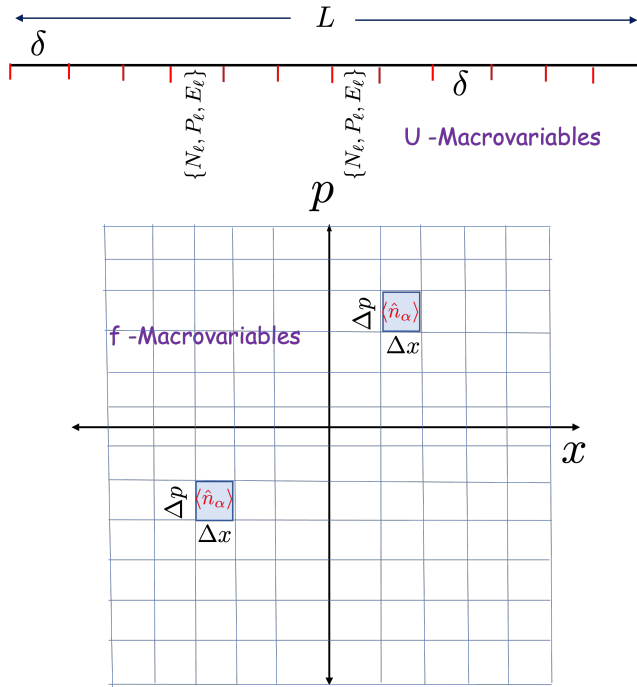$$S_{\mathrm{GvN}} = -k_B \, \mathrm{Tr}[\hat{\rho}_N \ln \hat{\rho}_N] \tag{6}$$

Fig. 1 Schematic of the macrovariables that we consider. (Top panel) U-macrovariables in which, the box of length L is divided into cells of length δ. By U-macrovariables, we mean coarse-grained particle number, momentum, and energy within each cell. (Bottom panel) f-macrovariables in which the macrovariables are defined by coarse-graining in the single-particle phase space. By f-macrovariables we mean coarse-grained particle numbers within each box of area $\Delta x \Delta p$. A macrostate corresponds to a specification of the values of the macrovariables.

over all $\hat{\rho}_N$, subject to the constraints $Tr[\hat{M}_k \hat{\rho}_N] = \langle \hat{M}_k \rangle$ [24].

Using this generalized canonical approach to compute the Boltzmann entropy permits more flexibility in the choice of macrovariables, as compared to those that adhere to the conditions needed for the above construction of generalized microcanonical macrostates. In particular, the spectra of the operators $\{\hat{M}_k\}$ need not be coarse-grained, and for quantum systems, these operators need not commute and may be microscopic operators, as we demonstrate in the example below.

3 An illustrative example: a one-dimensional quantum ideal gas

In this work, we consider a quantum ideal gas of N particles on a circle of length L. We examine the Boltzmann entropy for two different choices of macrovariables, schematically described in Fig. (1), that are quantum analogs of those used for the classical ideal gas in Ref. [15]:

1. U-macrovariables: These are specified by the three conserved fields of particle number, momentum, and energy and are direct analogs of the corresponding classical macrovari-

ables [15]. They correspond to the usual fields that are used in the hydrodynamic description of interacting systems — our non-interacting system has further conserved quantities but we can choose to consider the coarse-grained description in terms of these fields alone. More specifically, we divide our system of length L into A spatial cells of size $\delta = L/A$. We consider a set of operators $\{\hat{N}_\ell, \hat{P}_\ell, \hat{E}_\ell\}$, $\ell = 1, 2 \ldots A$, corresponding to the total number of particles, the total momentum, and the total energy in the ℓth cell. The precise definitions of these operators are given in Sec. (5.1). Given that the system is in a microstate $|\Phi(t)\rangle$, let $\langle\hat{B}\rangle = \langle\Phi|\hat{B}|\Phi\rangle$ denote the expectation value of any operator $\hat{B}$. Then, the set of expectation values $\{N_\ell, P_\ell, E_\ell\} = \{\langle\hat{N}_\ell\rangle, \langle\hat{P}_\ell\rangle, \langle\hat{E}_\ell\rangle\}$ specify, as we argued in the preceding paragraphs, the U-macrostate.

2. f-macrovariables: For the classical gas, the f-macrovariables are the distribution $f(x, p)$ of the single-particle positions and momenta [15]. Here we do not use a direct quantum analog of the classical macrovariables, but instead use a more microscopic choice, which is permitted for the quantum gas: We choose a complete and orthonormal basis of single-particle wavefunctions, each of which is approximately localized in position space within a width Δx and in momentum space with width Δp. Such states will necessarily have to satisfy the uncertainty relation $\Delta x \Delta p \gtrsim \hbar$. As we will show in Sec. (5.2), it is possible to construct such an orthonormal basis set on the circle with states that are approximately localized in position space with $\Delta x = L/K$ and in momentum space with $\Delta p = 2\pi\hbar K/L$, where K is an integer. We denote these single-particle basis states by $|\psi_\alpha\rangle$ with $\alpha \equiv (r, v)$, where $r = 1, \ldots, K$ and $v = \vartheta K$ where $\vartheta \in \mathbb{Z}$. These states are localized around $x = r\Delta x$ and $p = \vartheta\Delta p$. Let $\hat{n}_\alpha$ be the number operator corresponding to the occupation of the state $|\psi_\alpha\rangle$. The commuting operators $\{\hat{n}_\alpha\}$ form a set of *micro*variables, since specifying all of their eigenvalues specifies the microstate completely.

To define macrovariables for the quantum gas, we consider the expectation values $\{D_\alpha = \langle\hat{n}_\alpha\rangle\}$ in the microstate $|\Phi\rangle$. Since a pure state wavefunction of a quantum system implies a probabilistic description, specifying only the $\{D_\alpha\}$ implies a coarse-graining, in the sense that they do not specify the microstate. In fact, these expectation values $\{D_\alpha\}$ constitute a good set of macrovariables that can be used to define a corresponding generalized canonical ensemble and Boltzmann entropy, following the procedure outlined above. The resulting Boltzmann entropy is

$$S_{\text{B}}^f = \sum_\alpha \left[-D_\alpha \ln D_\alpha \mp (1 \mp D_\alpha) \ln(1 \mp D_\alpha) \right], \tag{7}$$

where the negative and positive signs in the $\mp$ are for fermions and bosons, respectively. This entropy can also be described from a generalized *grand* canonical ensemble, where each of the single-particle states α has its own chemical potential μ_α in order to set D_α. For the classical gas, the cells $\Delta x \Delta p$ used to define the f-macrovariables must be large enough so that they are typically occupied by many particles, in order to have enough coarse-graining [15]. For the quantum gas, on the other hand, fully microscopic cells may be used, and the needed coarse-graining is provided by using the expectation values as the macrovariables.

4 Microscopic model and dynamical evolution

Our system is a quantum ideal gas of N particles on a circle of length L. The microstate of the system is a pure state $|\Phi(t)\rangle$ or, using the position representation, the wavefunction $\Phi(x_1, x_2, \ldots, x_N, t)$. This state evolves in time via the Schrödinger equation $i\hbar\partial_t\Phi = \hat{H}\Phi$ with the free circle Hamiltonian $\hat{H} = -[\hbar^2/(2m)]\sum_{\ell=1}^{N}\partial_{x_\ell}^2$. The gas is initially confined to a part of the circle, of length aL with $0 < a < 1$ (usually $a = 1/2$), which we refer to as a "box". The initial N-particle state $|\Phi(0)\rangle$ may be taken to be an eigenstate of the occupations of the single-particle energy eigenstates in the box. We also compare our results to the initial grand canonical mixed states in the box. At $t = 0$, the box walls are removed at both ends and the gas is allowed to freely expand on the full circle. As the gas expands, we are interested in the time evolution of the macrovariables U and f and of the corresponding entropies.

The single-particle energy eigenstates and eigenvalues on the circle are given by

$$\varphi_n(x) = \frac{1}{\sqrt{L}}e^{2\pi inx/L} \text{ for } x \in [0, L), \tag{8}$$

$$\epsilon_n = \frac{1}{2m}\left(\frac{2\pi n\hbar}{L}\right)^2, \tag{9}$$

where n runs over all integers. These are also momentum eigenstates with eigenvalues $p_n = 2\pi n\hbar/L$. A complete N particle basis of Fock states is specified by the occupations $|\{N_n\}\rangle$ with $N_n \in \{0, 1\}$ for fermions and $N_n \in \{0, 1, \ldots, \infty\}$ for bosons, constrained so that $\sum_n N_n = N$. We will find it useful sometimes to use the language of second quantization and so we define the particle creation and annihilation operators $\hat{\Psi}^\dagger(x), \hat{\Psi}(x)$ which create or annihilate, respectively, a particle at position x. For fermions, they satisfy the anti-commutation relation $\{\hat{\Psi}(x), \hat{\Psi}^\dagger(x')\} = \delta(x - x')$, while for bosons they satisfy the commutation relation $[\hat{\Psi}(x), \hat{\Psi}^\dagger(x')] = \delta(x - x')$. We also define the creation and annihilation operators $\hat{b}_n^\dagger, \hat{b}_n$, corresponding to the single-particle energy eigenstate φ_n. These are related to the position operators as $\hat{\Psi}(x) = \sum_n \hat{b}_n\varphi_n(x)$. In the Heisenberg representation, these operators have simple time evolution for our noninteracting gas

$$\hat{b}_n(t) = e^{-i\epsilon_n t/\hbar}\hat{b}_n(0). \tag{10}$$

As we will see in the subsequent sections, for our purposes, it suffices to study the single-particle density matrix and the corresponding Wigner function. Therefore, in the following subsections, we discuss the evolution of the density matrix and the Wigner function.

4.1 Density matrix

For our analysis of the dynamics, we will use the single-particle density operator $\hat{\rho}_1$. In the Heisenberg picture, and in the basis of the single-particle energy eigenstates, $\hat{\rho}_1$ is a matrix of operators, with operator-valued matrix elements

$$\hat{\rho}_{1,mn}(t) \equiv \hat{\rho}_1(p_m, p_n, t) = \hat{b}_n^\dagger(t)\hat{b}_m(t) . \tag{11}$$

Note that this is normalized so $\sum_n \hat{\rho}_{1,nn}(t) = \hat{N}$ is the operator for the total particle number. In the position basis, the matrix elements of $\hat{\rho}_1(t)$ are given by

$$\rho_1(x, x', t) \equiv \langle x | \hat{\rho}_1(t) | x' \rangle = N \int dx_2 dx_3 \ldots dx_N$$

$$\Phi^*(x', x_2, x_3, \ldots x_N, t) \Phi(x, x_2, x_3, \ldots x_N, t)$$

$$= \mathrm{Tr}\left[\hat{\Psi}^\dagger(x')\hat{\Psi}(x)\hat{\rho}_N(t)\right], \tag{12}$$

where $\hat{\rho}_N(t)$ is the many-particle density matrix. For this given many-particle state $\hat{\rho}_N$, the single-particle density matrix is the matrix of expectation values of the single-particle density operator, which in the single-particle momentum eigenbasis we write as

$$\tilde{\rho}_1(p_m, p_n, t) \equiv \mathrm{Tr}\left[\hat{b}_n^\dagger(t)\hat{b}_m(t)\hat{\rho}_N\right]$$

$$\equiv \left\langle \hat{b}_n^\dagger(t)\hat{b}_m(t) \right\rangle = e^{-i(\epsilon_m - \epsilon_n)t/\hbar} \tilde{\rho}_1(p_m, p_n, 0). \tag{13}$$

Thus we can compute the evolution of $\hat{\rho}_1$ once we know the initial value, $\tilde{\rho}_1(p_m, p_n, 0)$, which we now evaluate.

For the description of the initial state where the gas is confined to a box of length aL, we will need the following single-particle "box" energy eigenspectrum

$$\chi_s(x) = \sqrt{\frac{2}{aL}} \sin \frac{s\pi x}{aL} \text{ for } x \in [0, aL], \tag{14}$$

$$e_s = \frac{\pi^2 \hbar^2 s^2}{2ma^2 L^2}, \tag{15}$$

where s runs over all positive integers. The box and circle states are related by the transformation

$$\chi_s(x) = \sum_{n=-\infty}^{\infty} V_{sn} \, \varphi_n(x), \tag{16a}$$

$$V_{sn} = \int_0^{aL} \chi_s(x)\varphi_n^\star(x)\, dx \tag{16b}$$

$$= \frac{\sqrt{2a}s}{\pi(4a^2 n^2 - s^2)}[e^{-2\pi i n a} \cos s\pi - 1].$$

Note that since $\{\chi_s(x), s = 1, \ldots, \infty\}$ do not form a complete set for states on the circle, V is not an invertible matrix.

As mentioned before, we are interested in the evolution of an N particle Fock state with energy E. For large N and E, it is equivalent and more convenient to work with a grand-canonical distribution with β and μ chosen according to

$$N = \sum_{s=1}^{\infty} f(e_s, \beta, \mu), \tag{17a}$$

$$E = \sum_{s=1}^{\infty} f(e_s, \beta, \mu)e_s, \tag{17b}$$

where $f(e, \beta, \mu) = \dfrac{1}{e^{\beta(e-\mu)} \pm 1}$ is the Fermi (+) /Bose (-) function.

In our numerical implementation, we use the following protocol. We prepare the system in a pure state with the single-particle density matrix given by

$$\hat{\rho}_1^{\mathrm{P}}(0) = \sum_{s=1}^{\infty} n_s \, |\chi_s\rangle\langle\chi_s|, \tag{18}$$

where the superscript "P" in Eq. (18) denotes pure state and the set $\{n_s\}$ is chosen from the grand-canonical distribution

$$P(\{n_s\}) = \frac{1}{Z} e^{-\beta \sum_s (e_s - \mu) n_s}, \tag{19}$$

$$Z = \prod_s [1 \pm e^{-\beta(e_s - \mu)}]^{\pm 1}, \tag{20}$$

subject to the constraints $\sum_s n_s = N$ and $\sum_s n_s e_s = E$. Here $n_s \in \{0, 1\}$ for fermions (+) and $n_s \in \{0, 1, \ldots, \infty\}$ for bosons (-). In practice, these constraints are difficult to satisfy exactly. Hence we chose the set $\{n_s\}$ such that these constraints are satisfied within some desired tolerance. We compare our results for the pure initial state with the mixed (thermal) state described by the single-particle density matrix

$$\hat{\rho}_1^{\mathrm{M}}(0) = \sum_{s=1}^{\infty} f(e_s, \beta, \mu) \, |\chi_s\rangle\langle\chi_s|, \tag{21}$$

where the superscript "M" in Eq. (21) denotes mixed thermal state. Using the box-to-circle transformation in Eq. (16a), we can write the density matrix in Eq. (21) in terms of the circle eigenfunctions to give

$$\tilde{\rho}_1^{\mathrm{M}}(p_m, p_n, 0) = \sum_{s=1}^{\infty} f(e_s, \beta, \mu) V_{sm} V_{sn}^{\star}. \tag{22}$$

Using Eq. (13), the evolution of the density matrix in Eq. (22) is thus given by:

$$\hat{\rho}_1^{\mathrm{M}}(t) = \sum_{s=1}^{\infty} f(e_s, \beta, \mu) \sum_{m,n=-\infty}^{\infty} V_{sm} V_{sn}^{\star} \, e^{-i(\epsilon_m - \epsilon_n)t/\hbar} \, |\varphi_m\rangle\langle\varphi_n|. \tag{23}$$

The pure state density matrix $\hat{\rho}_1^{\mathrm{P}}$ has a similar representation with $f(e_s, \beta, \mu)$ replaced by n_s in Eqs. (22) and (23). Note that the normalization condition $\operatorname{Tr} \hat{\rho}_1(t) = N$ implies $(VV^{\dagger})_{ss} = 1$. The density matrix in Eq. (23) and the corresponding representation of $\hat{\rho}_1^{\mathrm{P}}(t)$ are used to calculate local densities corresponding to conserved quantities.

4.2 Wigner distribution function

The Wigner distribution function (WDF) was introduced by Wigner [25, 26] as a quantum analogue of the phase space distribution in classical systems. In 1-d, on the infinite line, the WDF, denoted by $w(x, p, t)$, is defined as

$$w(x,p,t) = \frac{1}{2\pi\hbar} \int\limits_{-\infty}^{\infty} dy \, \rho_1\left(x + \frac{y}{2}, x - \frac{y}{2}, t\right) e^{ipy/\hbar}. \tag{24}$$

We point out that the above transformation is one-to-one, thus the WDF and the density matrix contain the same information. For noninteracting systems in the absence of external potentials, $w(x, p, t)$ satisfies the simple equation

$$\partial_t w(x,p,t) + \frac{p}{m} \partial_x w(x,p,t) = 0, \tag{25}$$

which is identical to the evolution equation of the single-particle phase space density in classical non-interacting systems. The solution of Eq .(25) is simply given by boosting the initial profile

$$w(x,p,t) = w\left(x - \frac{pt}{m}, p, 0\right). \tag{26}$$

In our model, the gas is confined to a circle of length L instead of the infinite line. Therefore, we have $x \in [0, L]$ and the allowed momenta, $p_n = 2\pi n\hbar/L$, with integer n, are discrete. A natural extension of the definition in Eq. (24) to the case of circular coordinates would be to replace p by p_n and restrict the integral from 0 to L [27, 28, 29]. However, this extension does not satisfy Eq. (25) with p replaced by p_n. It can be shown [30] that a modified definition of the WDF on the circle, that obeys Eq. (25), can be obtained. For this one needs to define a new momentum variable:

$$q_n = \frac{\pi n\hbar}{L} = \frac{p_n}{2}, \tag{27}$$

that takes both integer as well as half-integer values. The modified WDF on the circle is thus defined as

$$w(x, q_n, t) = \frac{1}{2L} \int\limits_{-L}^{L} dy \, \rho_1\left(x + \frac{y}{2}, x - \frac{y}{2}, t\right) e^{iq_n y/\hbar}, \tag{28}$$

$$= \frac{1}{L} \sum_{m=-\infty}^{\infty} \tilde{\rho}_1\left(q_n + \frac{p_m}{2}, q_n - \frac{p_m}{2}, t\right) e^{ip_m x/\hbar}, \tag{29}$$

where, in Eq. (29), the sum is over even values of m if q_n is an integer and odd values of m is q_n is a half-integer. The inverse transform is given by

$$\tilde{\rho}_1(p_m, p_n, t) = \int\limits_{0}^{L} dx \, w\left(x, \frac{p_m + p_n}{2}, t\right) e^{-i(p_m - p_n)x/\hbar}. \tag{30}$$

It is easy to check that the Wigner function in Eq. (28) satisfies Eq. (25) on the circle with p replaced by q_n and thus has a solution of the form in Eq. (26) with periodicity L. Using Eq. (23) in Eq. (29), we get

$$
\begin{aligned}
w(x, q_n, t) = \sum_{s=1}^{\infty} f(e_s, \beta, \mu) \sum_{\ell,m=-\infty}^{\infty} V_{s\ell} V_{sm}^{\star} \varphi_\ell(x) \varphi_m^{\star}(x) \\
\times\, e^{-i(\epsilon_\ell - \epsilon_m)t/\hbar} \delta(\ell + m - n),
\end{aligned}
\tag{31}
$$

for the mixed state and a similar expression for the pure state with $f(e_s, \beta, \mu)$ replaced by n_s. As we shall see in the next section, the WDF provides a simple way to define particle, momentum, and energy densities which are needed for defining the U-macrostate.

5 Choices of macrostates and the corresponding entropies

5.1 U-macrostate and S_B^U

In this section, we present the details of the construction of the U-macrostate. In this description, the observables that define the system's macrostate are the expectation values of the three conserved macroscopic fields, namely the particle, momentum, and energy densities. We first motivate the basic definition of the operators corresponding to these observables and then show that their expectation values can be written in a simple and physically intuitive form in terms of the WDF. We then discuss the corresponding entropy S_B^U.

Using second quantized notation, the operators corresponding to the total number of particles, total momentum, and total energy on the circle, in units of $\hbar = m = 1$, are given by

$$
\hat{N} = \int_0^L dx\, \hat{\Psi}^\dagger(x,t)\hat{\Psi}(x,t),
\tag{32a}
$$

$$
\hat{P} = -i \int_0^L dx\, \hat{\Psi}^\dagger(x,t)\partial_x\hat{\Psi}(x,t),
\tag{32b}
$$

$$
\hat{E} = -\frac{1}{2} \int_0^L dx\, \hat{\Psi}^\dagger(x,t)\partial_x^2\hat{\Psi}(x,t).
\tag{32c}
$$

It is then natural to define the following local density operators for the three fields:

$$
\hat{n}(x,t) = \hat{\Psi}^\dagger(x,t)\hat{\Psi}(x,t),
\tag{33a}
$$

$$
\hat{p}(x,t) = \frac{i}{2}\left[(\partial_x\Psi^\dagger(x,t))\Psi(x,t) - \Psi^\dagger(x,t)\partial_x\Psi(x,t)\right],
\tag{33b}
$$

$$
\begin{aligned}
\hat{e}(x,t) = -\frac{1}{8}\Big[&\hat{\Psi}^\dagger(x,t)\partial_x^2\hat{\Psi}(x,t) + (\partial_x^2\hat{\Psi}^\dagger(x,t))\hat{\Psi}(x,t) \\
&- 2(\partial_x\hat{\Psi}^\dagger(x,t))(\partial_x\hat{\Psi}(x,t))\Big].
\end{aligned}
\tag{33c}
$$

The forms above follow the requirement that the operators are self-adjoint, though, for the case of energy density, the choice is not unique. Our choice is motivated by the simple form it takes when we write the expectation value in terms of the WDF and it satisfies conditions on the form of the density profile, that we expect on physical grounds. To define our coarse-grained macrovariables, we divide the circle into A cells of size $\delta = L/A$ and label them by the index $\ell = 1, 2, \ldots, A$ with the ℓth cell beginning at $x = (\ell - 1)\delta$. Our macrovariables are then the set of operators

$$\{\hat{N}_\ell, \hat{P}_\ell, \hat{E}_\ell\} = \int\limits_{(\ell-1)\delta}^{\ell\delta} dx \{\hat{n}(x), \hat{p}(x), \hat{e}(x)\}. \tag{34}$$

To find the values of the macrovariables for a given microstate, we need the expectation values of the above operators. We find that the expectation values for the densities take the following simple forms when written in terms of the WDF:

$$n(x, t) = \sum_{n=-\infty}^{\infty} w(x, q_n, t), \tag{35a}$$

$$p(x, t) = \sum_{n=-\infty}^{\infty} q_n w(x, q_n, t), \tag{35b}$$

$$e(x, t) = \sum_{n=-\infty}^{\infty} (q_n^2/2) w(x, q_n, t). \tag{35c}$$

As is clear from the above equations, the densities take a physically intuitive form as the marginals of the Wigner function. The expectation values of the macrovariables in Eq. (34) are denoted by $\{N_\ell, P_\ell, E_\ell\}$ and are readily obtained by integrating Eq. (35) across cells.

Entropy of the U-macrostate: We now return to our goal of defining the entropy for the U-macrostate. Given the set $\{N_\ell, P_\ell, E_\ell\}$, $\ell = 1, 2, \ldots, A$, we need to find the number of microstates consistent with a given specification for the values of the set. Assuming small correlations between cells, the number of microstates with these constraints is simply the product of the number of possible microstates in each cell (with the local constraints). Hence we get for the entropy

$$S_B^U = \sum_{\ell=1}^{A} S(N_\ell, P_\ell, E_\ell), \tag{36}$$

where $S(N_\ell, P_\ell, E_\ell)$ is the equilibrium entropy of the ℓth cell of size $\delta = L/A$ with the specified values of the conserved quantities N_ℓ, P_ℓ, E_ℓ.

5.2 f-macrostate and S_B^f

As discussed in Sec. (2) the construction of the f-macrostate requires us to find a basis set of single particle wavefunctions that are localized both in position and momentum space.

We now discuss its construction. The φ-basis, defined in Eq. (8), consists of momentum eigenstates on the circle that are completely delocalized in position space. To construct our localized basis, we superimpose K number of successive φ-states labelled by a central momentum $p = 2\pi\hbar v/L$, and generate K new states

$$|\psi_\alpha\rangle \equiv |r, v\rangle = \frac{1}{\sqrt{K}} \sum_{n \,\epsilon\, \mathscr{R}_v} |\varphi_n\rangle \, e^{-in\frac{2\pi r}{K}}, \tag{37}$$

where $\mathscr{R}_v = \{v - (K-1)/2, \ldots, v + (K-1)/2\}$ and $\alpha \equiv (r, v)$ is a collective index for the basis states. Note that $r = 1, \ldots, K$ and $v = \vartheta K$ where ϑ takes all integer values. The K resulting $|r, v\rangle$ states for a given v are localized around rL/K, $r = 1, \ldots, K$ in the position space and around $2\pi\hbar v/L$ in the momentum space. For this reason, we shall refer to the ψ-basis in Eq. (37) as the *wavepacket basis*.

We now define the *wavepacket density*, denoted by $D_\alpha(t) = \langle \hat{n}_\alpha \rangle \equiv D(r, v, t)$, as the diagonal of the single-particle density matrix $\hat{\rho}_1(t)$ in the wavepacket basis

$$D_\alpha(t) \equiv D(r, v, t) = \langle r, v| \, \hat{\rho}_1(t) \, |r, v\rangle. \tag{38}$$

It turns out that one can write down the wavepacket density in terms of the Wigner function as

$$D(r, v, t) = \frac{1}{K} \sum_{\ell, m \in \mathscr{R}_v} \int_0^L dx \, w\left(x, \frac{\ell + m}{2}, t\right) e^{-2\pi i(\ell - m)z}, \tag{39}$$

where $z = x/L - r/K$. Making the variable transformation $q = (\ell + m)/2$ and $n = \ell - m$, we can rewrite Eq. (39) as

$$D(r, v, t) = \frac{1}{K} \sum_{q=v_-}^{v_+} \int_0^L dx \, w(x, q, t) \sum_{n=2(q-v_+)}^{2(q-v_-)} e^{-2\pi inz}, \tag{40}$$

where $v_\pm = v \pm (K-1)/2$. Summing over n yields

$$D(r, v, t) = \frac{1}{K} \sum_{q=v_-}^{v_+} \int_0^L dx \, w(x, q, t) G_K(q - v, x), \tag{41}$$

$$G_K(q, x) = e^{-4\pi iqz} \frac{\sin(2K-1)\pi z}{\sin \pi z}, \tag{42}$$

where recall $z = x/L - r/K$. Eq. (41) suggests that the wavepacket density is nothing but a coarse-grained WDF. It is also instructive to look at the marginals of the wavepacket density. The momentum marginal is given by the expression (see Appendix A)

$$D_v(v) = \sum_{r=1}^K D(r, v, t) = \sum_{n \in \mathscr{R}_v} \tilde{\rho}_1(p_n, p_n, 0), \tag{43}$$

where recall $\mathscr{R}_v$ denotes set of momenta centered around v. Similarly, the position marginal is given by (see Appendix A)

$$D_r(r,t) = \sum_v D(r,v,t) = \int_0^L dx\, h_K\left(\frac{x}{L} - \frac{r}{K}\right)\rho_1(x,x,t), \tag{44}$$

$$\text{with } h_K(x) = \frac{1}{K^2}\left(\frac{\sin \pi K z}{\sin \pi z}\right)^2. \tag{45}$$

Note that Eqs. (43, 44) represent coarse-grained versions of the diagonal elements of the density matrix in the momentum and position basis.

Entropy of the f-macrostate: We now discuss the entropy formula in Eq. (7) for a given specification of the set $\{D_\alpha\}$. To derive this formula, one maximizes the Gibbs-von Neumann entropy, $S_{\text{GvN}} = -\text{Tr}[\hat{\rho}_N \log \hat{\rho}_N]$, subject to the constraint

$$D_\alpha(t) = \langle\psi_\alpha|\,\hat{\rho}_1(t)\,|\psi_\alpha\rangle = \text{Tr}\left[\hat{\rho}_N(t)\hat{\Psi}_\alpha^\dagger\hat{\Psi}_\alpha\right], \tag{46}$$

where $\hat{\Psi}_\alpha$ creates a particle in the state $|\psi_\alpha\rangle$. The density matrix $\hat{\rho}_N^\star$ that maximizes S_{GvN} is given by

$$\hat{\rho}_N^\star = \frac{1}{Z}\,e^{-\sum_\alpha \lambda_\alpha \hat{\Psi}_\alpha^\dagger\hat{\Psi}_\alpha}, \tag{47}$$

$$Z = \prod_\alpha [1 \pm e^{-\lambda_\alpha}]^{\pm 1}, \tag{48}$$

where $+$ is for fermions and $-$ is for bosons. Note that this is precisely the density matrix that defines the equivalent generalized canonical ensemble $\hat{\rho}_{GC}$, as mentioned in Sec. (2). The Lagrange multipliers λ_α are given by the relation

$$D_\alpha = \text{Tr}\left[\hat{\rho}_N^\star\hat{\Psi}_\alpha^\dagger\hat{\Psi}_\alpha\right] = \frac{1}{e^{\lambda_\alpha} \pm 1}. \tag{49}$$

We can thus write down the maximal Gibbs-von Neumann entropy, $S_B^f = -\text{Tr}[\hat{\rho}_N^\star \log \hat{\rho}_N^\star]$, in terms of D_α as

$$S_B^f = \sum_\alpha \left[-D_\alpha \ln D_\alpha \mp (1 \mp D_\alpha)\ln(1 \mp D_\alpha)\right], \tag{50}$$

where the $-$ in the $\mp$ is for fermions and the $+$ is for bosons.

In order to compute the final change in entropy $\Delta s_B^f = (S_B^f(\infty) - S_B^f(0))/N$, we next provide analytical estimates for the values of $D_\alpha(t)$ at $t \to \infty$ and $t = 0$. Substituting the expression for $\hat{\rho}_1(t)$ from Eq. (23) into Eq. (38), we obtain an explicit expression for the wavepacket density

$$D_\alpha(t) = \sum_{s=1}^\infty f(e_s, \beta, \mu)\sum_{m,n=-\infty}^\infty V_{sm}V_{sn}^\star e^{-i(\epsilon_m - \epsilon_n)t/\hbar}\langle\psi_\alpha|\varphi_m\rangle\langle\varphi_n|\psi_\alpha\rangle. \tag{51}$$

We first discuss the late time limit. As $t \to \infty$, we only get contributions from the $m = n$ terms in Eq. (51)

$$D_\alpha(\infty) = \sum_{s=1}^{\infty} f(e_s, \beta, \mu) \sum_{n=-\infty}^{\infty} |V_{sn}|^2 \, ||\langle \varphi_n | \psi_\alpha \rangle||^2. \tag{52}$$

In the limit of large N and L (keeping $N/L = \rho$ fixed), we use the explicit form of V_{sn} in Eq. (16b) and find that $|V_{sn}|^2$ is highly peaked around $s \approx 2an$ for large n. Hence the sum can be approximated as $\sum_s f(e_s, \beta, \mu) |V_{sn}|^2 \approx f(e_{2an}, \beta, \mu) \sum_s |V_{sn}|^2 = af(\epsilon_n, \beta, \mu)$. We thus get for the late time

$$D_\alpha(\infty) = \frac{a}{K} \sum_{n=\mathscr{R}_v} f(\epsilon_n, \beta, \mu). \tag{53}$$

To compute $D_\alpha(0)$ we start with the expression

$$D_\alpha(0) = \sum_{s=1}^{\infty} f(e_s, \beta, \mu) \sum_{m,n=-\infty}^{\infty} V_{sm} V_{sn}^{\star} \langle \psi_\alpha | \varphi_m \rangle \langle \varphi_n | \psi_\alpha \rangle. \tag{54}$$

Using Eq. (16b) for V_{sm}, we obtain the following simplified form:

$$D_\alpha(0) = \frac{1}{K} \sum_{s=1}^{\infty} f(e_s, \beta, \mu) |g_v(s, r)|^2, \text{ where} \tag{55}$$

$$g_v(s, r) = \sqrt{\frac{2}{a}} \int_{-r/K}^{a-r/K} dz \sin\left[\frac{s\pi}{a}\left(z + \frac{r}{K}\right)\right] e^{-2\pi i v z} \frac{\sin \pi K z}{\sin \pi z}. \tag{56}$$

Since the integrand in $g_v(s, r)$ is highly peaked about $z = 0$ for large K, we make the replacement $\sin(\pi z) \approx \pi z$ in the numerator whenever $z = 0$ falls inside the integration limit *i.e.* for $r < Ka$. This allows us to make the following approximation $g_v(s, r) \approx \Theta(Ka - r)\tilde{g}_v(s, r)$ where $\Theta(r)$ is the Heaviside Theta function and $\tilde{g}_v(s, r)$ is given by

$$\tilde{g}_v(s, r) \approx \sqrt{\frac{2}{a}} \int_{-\infty}^{\infty} dz \sin\left[\frac{s\pi}{a}\left(z + \frac{r}{K}\right)\right] e^{-2\pi i v z} \frac{\sin \pi K z}{\pi z}. \tag{57}$$

This finally implies

$$|\tilde{g}_v(s, r)|^2 \approx \frac{1}{2a}\Theta(s_+ - s)\Theta(s - s_-), \tag{58}$$

with $s_\pm = 2av \pm Ka$. Using this approximation in Eq. (55), we get

$$D_\alpha(0) \approx \frac{1}{2aK} \sum_{s=s_-}^{s_+} f(e_s, \beta, \mu)\Theta(r < Ka). \tag{59}$$

Note that while making the above approximations, we have ignored possible r dependence near the edges of the initial box of size aL. As a result, the approximated density $D_\alpha(0)$ slightly underestimates the initial entropy.

Using $D_\alpha(\infty)$ from Eq. (53) and $D_\alpha(0)$ from Eq. (59), in Eq. (50) one can numerically compute Δs_B^f for different T and μ. However the above procedure does not remain valid

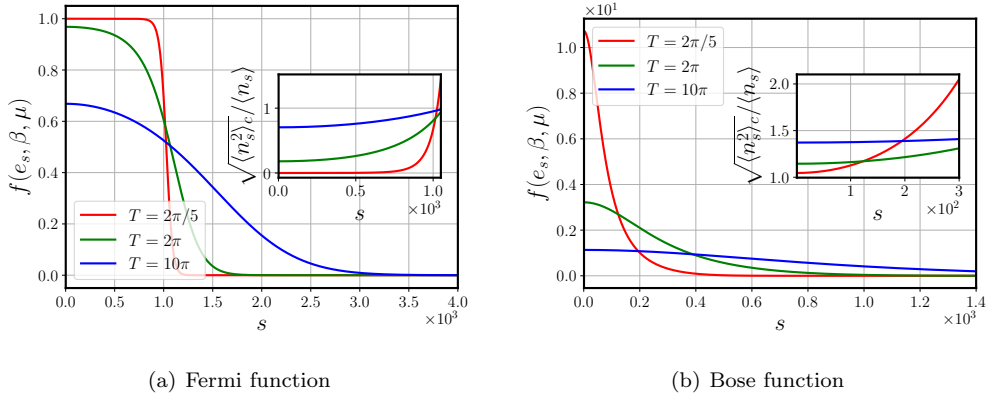(a) Fermi function   (b) Bose function

Fig. 2 Fermi and Bose distribution functions showing the mean occupation numbers of energy levels at the low and high temperatures (along with an intermediate temperature for comparison) used in our numerical study. The particle density was set to $\rho = 1$. The insets show the relative number fluctuations.

for bosons at very low temperatures because the particles occupy only a few low-lying energy states and consequently they do not relax. On the other hand for fermions, the above procedure works for all T, and specifically at $T = 0$, one can obtain an explicit expression of Δs_B^f. To obtain this expression we first note that for $T = 0$, Eq. (53) gives $D_\alpha(\infty) = a$ for all α except those which are very close to the Fermi surface. Using $D_\alpha(\infty) \approx a$ in Eq. (50), we find

$$S_B^f(\infty) = -\sum_\alpha [a \ln a + (1 - a) \ln(1 - a)], \tag{60}$$

where the summation extends over $2n_{max}$ terms such that $\epsilon_{n_{max}} = \mu$. Given that $e_s = \epsilon_{s/2a}$ and $e_N = \mu$, we get $n_{max} = N/2a$. The number of terms in the α-sum is thus N/a and hence, the late time entropy per particle is given by

$$s_B^f(\infty) = -\frac{1}{a}[a \ln a + (1 - a) \ln(1 - a)]. \tag{61}$$

For $a = 1/2$, we obtain $s_B^f(\infty) = 2 \ln 2$. The initial density in Eq. (59) simplifies in a similar manner and we get

$$D_\alpha(0) = \frac{1}{2aK} \sum_{s=s_-}^{s_+} \Theta(e_s < \mu) \approx 1, \tag{62}$$

which results in the initial entropy at $T = 0$ being zero (neglecting edge contributions as mentioned earlier). We therefore get $\Delta s_B^f(T = 0) = 2 \ln 2$ for the Fermi gas expanding to twice the initial volume.

6 Numerical results

In this section, we present the results of the evolution of the two macrovariables f and U, and the corresponding entropies for fermions in Sec. (6.1) and for bosons in Sec. (6.2).

(a) $T = 2\pi/5$, $\mu = 19.84$

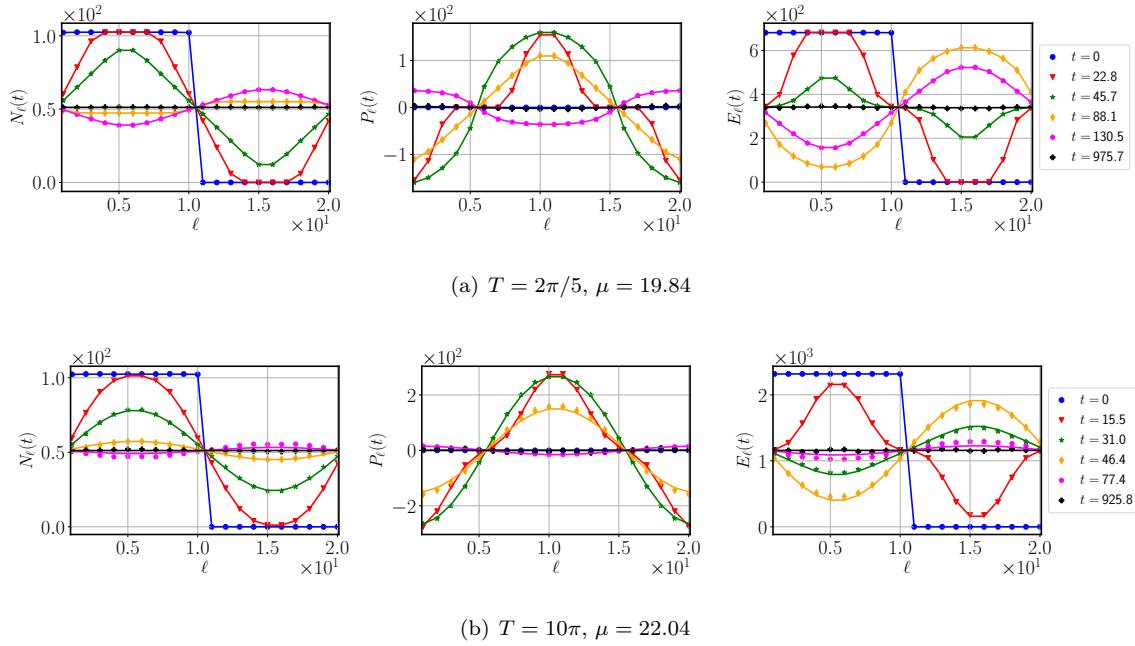(b) $T = 10\pi$, $\mu = 22.04$

Fig. 3 Fermions - evolution of U-macrovariables: Plots showing the spatial profiles of the number of particles, the total momentum, and the total energy in each of the $A = 20$ cells for $N = L = 1024$ at different times. The dots represent results for the pure state initial condition while the solid lines correspond to a thermal mixed state. Results are presented for two different temperatures $T = 2\pi/5$, 10π (top and bottom row respectively), and chemical potentials are fixed so that the mean density is set at $\rho = 1$. We see a good agreement between the pure state and the thermal state results.

The equilibrium state of an ideal gas is described by its temperature T and density $\rho = N/L$. For a quantum system, a relevant parameter that tells us whether we are in the quantum or classical regime is the ratio of the interparticle distance $1/\rho$ to the thermal de Broglie wavelength, $\lambda_{\text{th}} = h/(2\pi m k_B T)^{1/2}$. With our choice of units with $m = k_B = \hbar = 1$ and density fixed at $\rho = 1$, we take the square of this ratio, $(\lambda_{\text{th}}\rho)^{-2} = T/(2\pi)$ to be the controlling parameter. In the following, we will present results for two sets of parameters: (i) low-temperature highly quantum regime $T = 2\pi/5$; (ii) high-temperature regime $T = 10\pi$. In Fig. (2) we show the mean energy-level occupation number and their fluctuations for fermions and bosons at different temperatures.

We recall the two different initial conditions [see Sec. (4.1)] for which we present our results.

1. We consider the initial state to be a single pure many-body Fock state given by the box eigenstate:

$$|\Phi\rangle = |\{n_s\}\rangle \,, \tag{63}$$

where the single-particle level box occupancies, $\{n_s\}$, are chosen with probabilities given by the grand-canonical distribution [in the box $x \in (0, L/2)$] with T, μ fixed at the
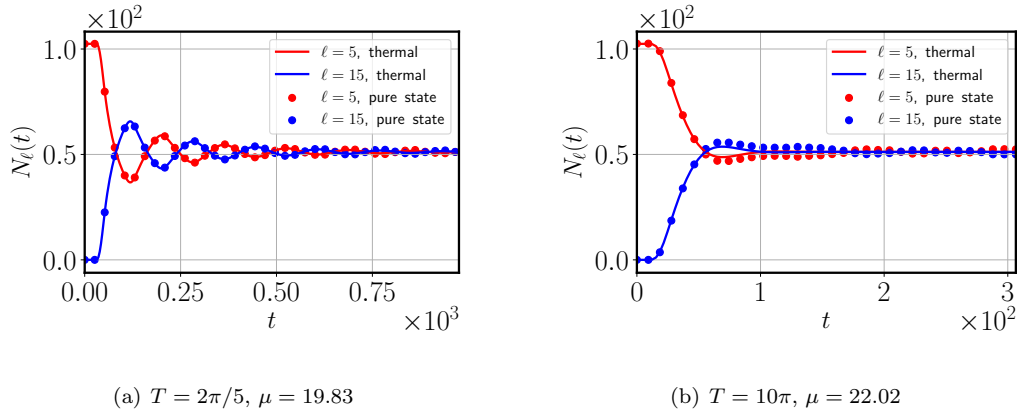
(a) $T = 2\pi/5$, $\mu = 19.83$ (b) $T = 10\pi$, $\mu = 22.02$

Fig. 4 Fermions: Time evolution of the number of particles inside the 5th and 15th cells out of a total of $A = 20$ cells for $N = L = 1024$. As in Fig. (3), we see a good agreement between the pure state (dots) and the thermal state results (solid line). We see marked oscillations at low temperatures with a time period $\tau_p = L/v_f$ (see text).

     desired values corresponding to our specified initial T, ρ. We sample only one initial state this way; for large N, this comes close to "self-averaging".
2. We consider an initial state whose one-particle density matrix is identical to that of the grand-canonical distribution in the box.

6.1 Fermions

In this section, we present results for fermions first for the U-macrovariable and then for the f-macrovariable.

6.1.1 U-macrostate

In this case, we set $L = N = 1024$ in all our numerics. Some of our main observations are:

(i) In Fig. (3) we show the spatial profiles of the U-macrovariables, given by the expectation values of the operators in Eq. (34), at different times starting with the gas in the region $(0, L/2)$ and with $A = 20$ partitions of the system. Results are shown for both the pure state and the thermal state initial conditions and we find a very good agreement between the two. We observe that at late times, all three fields approach uniform profiles which characterize our equilibrium state.

(ii) In Fig. (4) we consider two fixed cells centered at $x = L/4$ and $3L/4$ and plot the time-evolution of the number of particles in these cells. We again see a good agreement between the pure state and the thermal state initial conditions. An oscillatory relaxation to the uniform equilibrium state is observed. We note that the oscillation period in the low-temperature limit is given by $\tau_p = L/v_{\mathrm{f}}$ where v_{f} is the Fermi velocity. The amplitude of the oscillations decreases with increasing temperature.

(a) $T = 2\pi/5$, $\mu = 19.83$, $\Delta s = 1.46$ (b) $T = 10\pi$, $\mu = 22.02$, $\Delta s = 0.88$
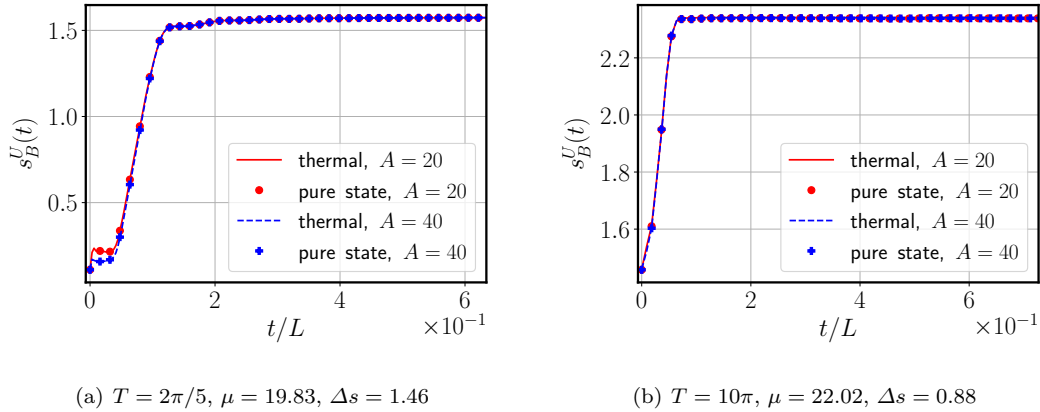
Fig. 5 Fermions: U-macrostate entropy growth for fermions for $N = L = 1024$ at two different temperatures and for two different coarse-graining scales with $A = 20$ (blue lines) and $A = 40$ (red lines). Results are presented for the pure state (dots) and thermal state (solid lines) initial conditions. The initial sharp rise corresponds to the filling of the two empty cells on either side of the unfilled part of the circle. This jump is smaller for finer coarse-graining size. We also observe an initial flat profile in (a) which persists till time $(L/4)/v_f$, where v_f is the Fermi velocity. At large times, in all cases, the entropy saturates to the thermodynamic entropy of the new equilibrium state (corresponding to uniform values of the three conserved fields on the circle). The sub-captions give the values for the change in entropy per particle, Δs, for the two cases.

(iii) The evolution of the Boltzmann entropy S_B^U at the two temperatures are shown in Fig. (5), for two choices of cell sizes, with $A = 20, 40$. We see a convergence of the growth curve with decreasing cell size. A monotonic growth of the entropy and an eventual saturation to the expected equilibrium value (corresponding to uniform values of the conserved fields) is observed. In the low-temperature case, we observe an initial jump in the S_B^U followed by a small flat regime and then a sharp increase. The initial jump size is smaller for finer coarse-graining. On the other hand, the initial flat profile seen in Fig. (5)(a) is a result of the sharp cutoff in the momentum distribution in the low-temperature Fermi gas. The flat region is observed till time $(L/4)/v_f$, where v_f is the Fermi velocity, which corresponds to the time taken by the gas to fill the circle for the first time.

6.1.2 f-macrostate

In this case, we set $L = N = 2048$ in all our numerics. Some of our main observations are:

(i) To see the evolution of the f-macrovariables, we plot heat maps in the top left of Fig. (6) showing the values of wavepacket density D_α in the two-dimensional $\alpha = (r, v)$ plane for an intermediate temperature $T = 2\pi$. We present six different time snapshots indicated by (a)-(e). The wavepacket density is initially flat in the box and there is an oscillatory relaxation to an eventual flat profile over the circle. We see an interference pattern that disappears in (d) and reappears in (e) and then again disappears in (f). This feature is more manifest in the top right panel of Fig. (6) which shows the wave packet density
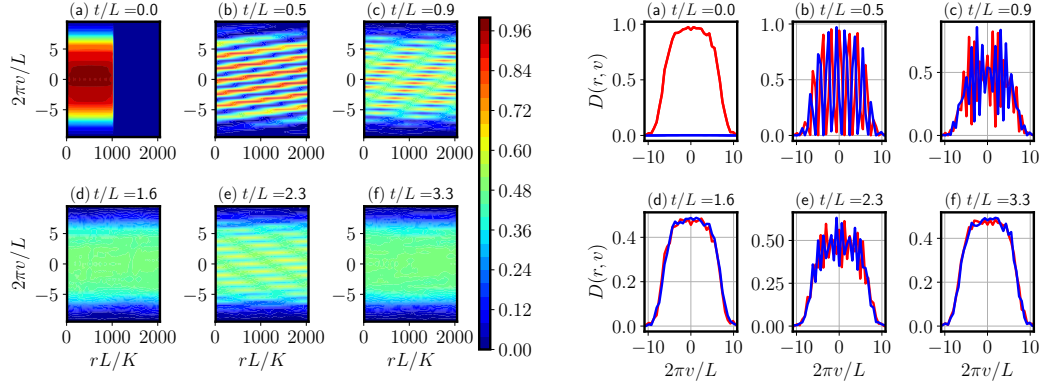
Fig. 6 Fermions - evolution of f-macrovariables. Top left: Heat map plot of the wave packet density for parameters $T = 2\pi$, $\mu = 21.53$, $N = L = 2048$, and $K = 201$. Top right: The wave packet density as a function of momentum at two values of $r = K/4$ (red) and $r = 3K/4$ (blue), at the same time instances as in the heat map. Bottom left: The entropy evolution with time where the points $a - f$ correspond to the same time snapshots as in the top row. The relative values of the entropy at these points are consistent with the presence of structures (or lack thereof) in the heat map and the cross-sectional profiles.
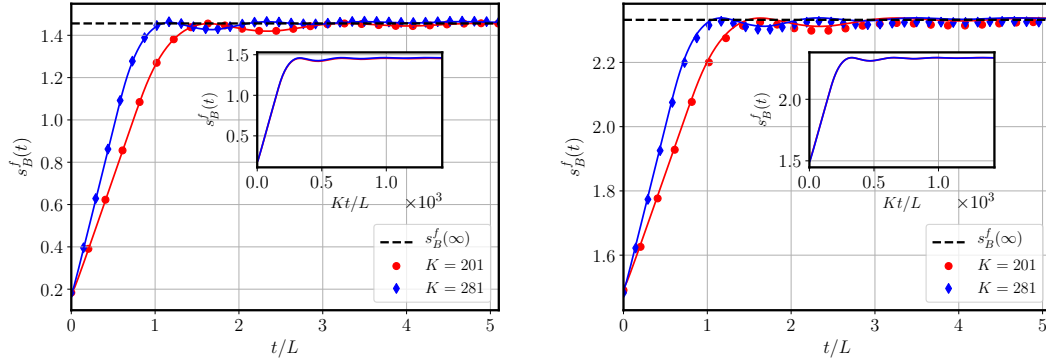
(a) $T = 2\pi/5$, $\mu = 19.82$, $\Delta s = 1.28$

(b) $T = 10\pi$, $\mu = 22.01$, $\Delta s = 0.84$

Fig. 7 Fermions: Time evolution of the f-macrostate entropy per particle, s_B^f, at two different temperatures and for two coarse-graining scales K at each temperature. We see very good agreement between results for the pure state (red dots) and thermal state (solid lines) initial conditions. The inset in each plot shows the collapse of different K curves on re-scaling time.

as a function of momentum at two values of $r = K/4$ (red) and $r = 3K/4$ (blue), at the same time instances as in the heat map. These features lead to an oscillatory relaxation of the entropy growth curve as seen in the bottom left panel of Fig. (6) where we find that the time for the entropy to first reach the saturation value, i.e, the point (d) is given by $L^2/(2\pi K)$. This is also the period of the subsequent oscillations seen in the entropy evolution. This time scale can be understood within a semi-classical framework and using the results from Ref. [15]. There it was shown that the time scale of oscillations of s_B^f is given by $\tau = L/\Delta v$, where Δv is the momentum coarse-graining scale. In the quantum case, we replace this by $\Delta v = \Delta p/m = 2\pi\hbar K/(mL)$. With our choice of units $\hbar = m = 1$, we therefore get $\tau = L^2/(2\pi K)$.

(ii) In Fig. (7), we plot the entropy growth for the two temperatures (low and high) and for two different K values corresponding to each temperature. At both coarse graining scales, K, we see a good agreement between the entropy calculated from the pure state and the thermal state initial conditions. The entropy saturates to a value as predicted from Eqs. (50, 53). In the inset, we see a collapse of the data for different K on scaling time by K, consistent with the expression for τ mentioned above. Note that similar oscillations and collapse of data were seen in the entropy growth in the free expansion of the non-interacting classical ideal gas [15].

6.2 Bosons

We now present results for bosons for the U and f macrovariables. Except at very low temperatures, we find that several features are the same as that of fermions irrespective of the difference in statistics. We also highlight the striking differences between bosons and fermions. For bosons at very low temperatures, only levels with the energy of order $\lesssim k_B T$ will be occupied. The number of occupied levels is thus small unless we consider very large N. Therefore it is difficult to see relaxation at such low temperatures and we do not consider such temperatures.

6.2.1 U-macrostate

In Fig. (8) we show the spatial profiles of the U-macrovariables, given by the expectation values of the operators in Eq. (34), at different times starting with the gas in the left half of the box. We again consider a partition of the box into $A = 20$ cells. Results are shown for both the pure state and the thermal state initial conditions and as before we find reasonable agreement between the two though we find significant differences at long times. In general, we find that for bosons the agreement is not as good as that of fermions due to stronger finite size effects. This is because, for a fixed total particle number and temperature, the typical number of occupied levels in the pure state is less for bosons compared to that for fermions and fluctuations are larger [see Fig. (2)].

In Fig. (9) we consider two fixed cells located on the two halves of the circle centered at $x = L/4$ and $3L/4$ and plot the time-evolution of the number of particles inside these cells. We again see a reasonable agreement between the results from the pure and thermal states, though the differences are significantly larger than what was seen for fermions. It is worth noting that unlike in the case of fermions, here we do not see any oscillations but rather a
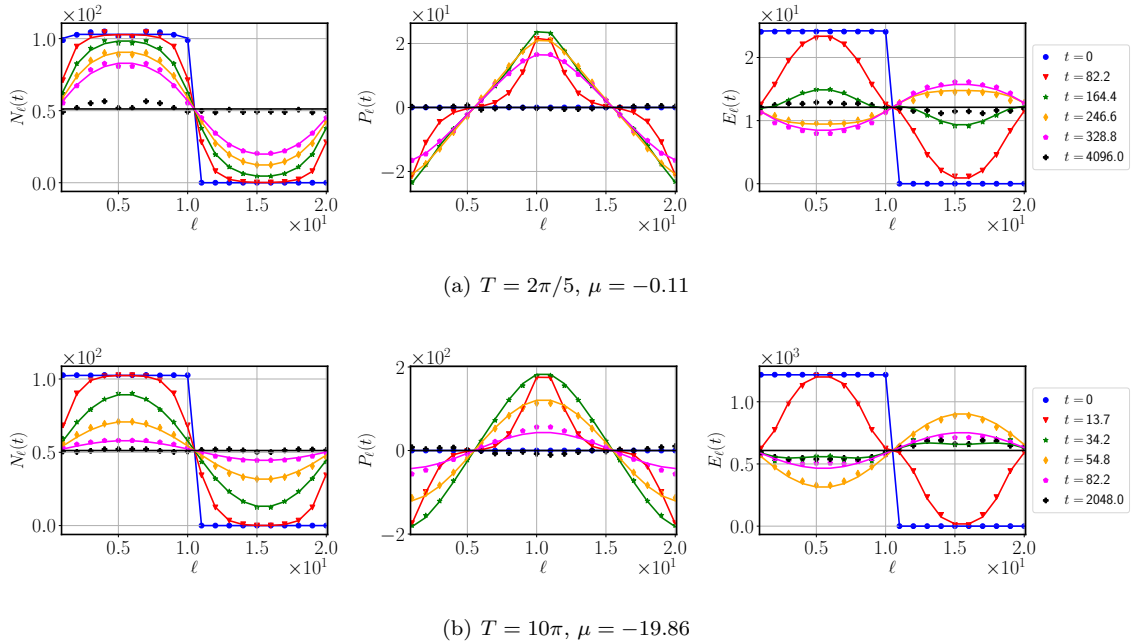
(a) $T = 2\pi/5$, $\mu = -0.11$

(b) $T = 10\pi$, $\mu = -19.86$

Fig. 8 Bosons - evolution of U-macrovariables: Plots showing the spatial profiles of the number of particles, the total momentum, and the total energy in each of the $A = 20$ cells for $N = L = 1024$ at different times. Results are presented for two different temperatures $T = 2\pi/5$, 10π, and chemical potentials are fixed so that the mean density is set at $\rho = 1$. We see a reasonable agreement between the pure state (red dots) and the thermal state (solid lines) results, but significant deviations (due to finite-size effects) are observed at the latest times.

monotonic relaxation to the uniform equilibrium state. The oscillations in the fermionic case arise due to the sharpness of the distribution near the Fermi energy at low temperatures which allows one to define a typical velocity v_F – hence a period of oscillation $\tau_p = L/v_F$. On the other hand in the case of bosons, we cannot identify such a typical velocity. Note that even though the evolution equation for the Wigner function is formally identical for bosons and fermions (as also classical particles), differences arise due to the form of the initial conditions. More precisely, for a typical pure state corresponding to thermal equilibrium, the form of the initial state is entirely different for bosons and fermions. The evolution of the Boltzmann entropy per particle s_B^U at the two temperatures is shown in Fig. (10), for two choices of cell sizes $A = 20, 40$. We observe: (i) a convergence of the growth curve with decreasing cell size; (ii) a monotonic growth of the entropy and an eventual saturation to the expected equilibrium value (corresponding to uniform values of the conserved fields).

6.2.2 f-macrostate

For the f-macrostate, we again plot the heat map of the wavepacket density and the corresponding entropy growth curve in Fig. (11). The results look similar to fermions, except for the fact that the wavepacket density for bosons is more smeared out as compared to
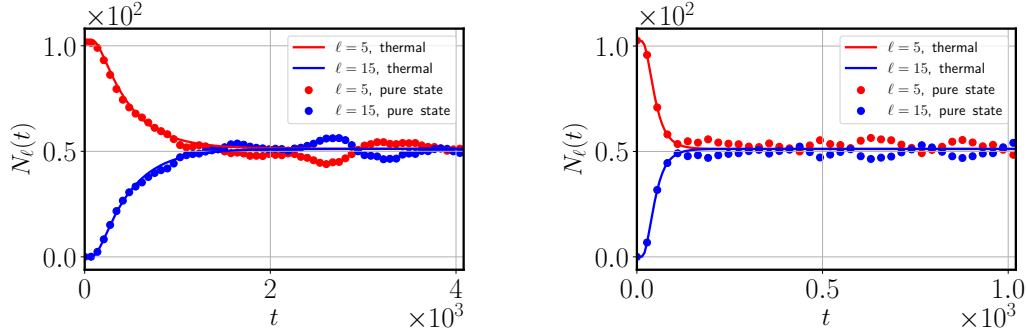
(a) $T = 2\pi/5$, $\mu = -0.11$, $N = L = 1024$ (b) $T = 10\pi$, $\mu = -19.85$, $N = L = 1024$

Fig. 9 Bosons: Time evolution of the number of particles inside the 5th and 15th cells out of a total of $A = 20$ cells for $N = L = 1024$. As in Fig. (8), we see a reasonable agreement, at early times, between the pure state (dots) and the thermal state results (solid line) while at longer times there are significant deviations. Note that the thermal data shows the absence of oscillations while in the pure state data, we see fluctuations that are expected to decrease with increasing system size.
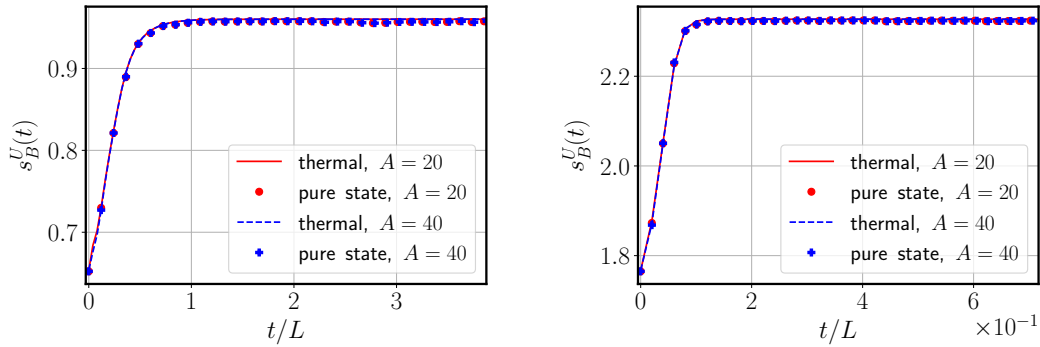

(a) $T = 2\pi/5$, $\mu = -0.11$, $\Delta s = 0.31$ (b) $T = 10\pi$, $\mu = -19.86$, $\Delta s = 0.56$

Fig. 10 Bosons: U-macrostate entropy growth for $N = L = 1024$ at two different temperatures and for two different coarse-graining scales with $A = 20$ (blue lines) and $A = 40$ (red lines). Results are presented for the pure state (dots) and thermal state (solid lines) initial conditions. Unlike for fermions, the initial sharp rise is not seen in the case of bosons. At large times, in all cases, the entropy saturates to the thermodynamic entropy of the new equilibrium state (corresponding to uniform values of the three conserved fields on the circle). The sub-captions give the values for the change in entropy per particle, Δs, for the two cases.

fermions. This is due to the usual difference between the Bose and the Fermi function at low temperatures. However, in the entropy growth curves for bosons in Fig (12), the saturation value of the entropy depends rather strongly on K, especially in the low-temperature case [see details in appendix (B)].
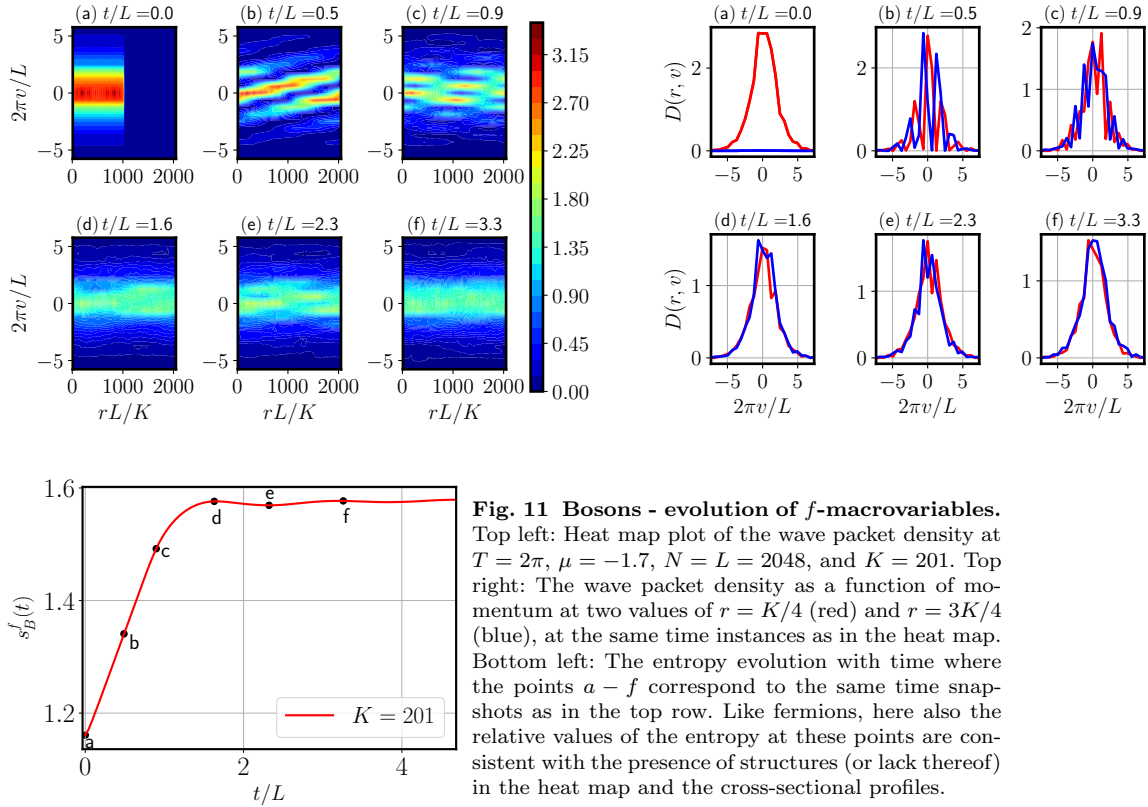
Fig. 11 Bosons - evolution of f-macrovariables. Top left: Heat map plot of the wave packet density at $T = 2\pi$, $\mu = -1.7$, $N = L = 2048$, and $K = 201$. Top right: The wave packet density as a function of momentum at two values of $r = K/4$ (red) and $r = 3K/4$ (blue), at the same time instances as in the heat map. Bottom left: The entropy evolution with time where the points $a - f$ correspond to the same time snapshots as in the top row. Like fermions, here also the relative values of the entropy at these points are consistent with the presence of structures (or lack thereof) in the heat map and the cross-sectional profiles.

7 Discussions and Conclusions

The main aim of this paper has been to use Boltzmann's ideas to construct an entropy function that can be defined for a pure quantum state and which allows us to characterize irreversibility in macroscopic systems. For the example of the quantum ideal gas, two sets of macroscopic descriptions (called U and f) were defined that provide a coarse-grained view of the system, which is in a pure quantum state. The evolution of the entropy functions associated with these macrostates was studied for the case where the gas, initially in a pure state and spatially confined, was allowed to expand to twice its volume. We summarize and comment on some of our main results.

1. The U-macrovariables are the coarse-grained operators corresponding to the number, momentum, and energy of particles in spatial cells of size $\delta = L/A$. For both fermions and bosons, we see that the macrostates reach a steady state characterized by the three fields reaching homogeneous spatial profiles. Depending on the parameter values, we see either damped or oscillatory relaxation of the fields to the steady state. However, we always observe a monotonic increase of the associated entropy, s_B^U.
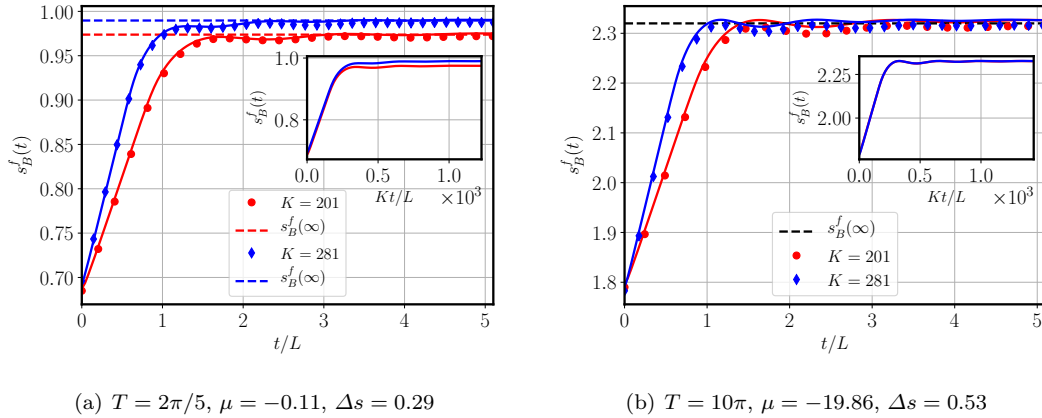
(a) $T = 2\pi/5$, $\mu = -0.11$, $\Delta s = 0.29$ (b) $T = 10\pi$, $\mu = -19.86$, $\Delta s = 0.53$

Fig. 12 Bosons: Time evolution of the f-macrostate entropy per particle, s_B^f, at two different temperatures and for two coarse-graining scales K at each temperature. We see a good agreement between results for the pure state (red dots) and thermal state (solid lines) initial conditions. The inset in each plot shows the collapse of different K curves on re-scaling time.

2. The definition of our f-macrostate is aimed at obtaining an analogue of the single-particle phase space density in classical systems. A natural candidate for this are the number operators corresponding to a localized wavepacket set of basis states. While these operators are not bonafide macrovariables, we nevertheless can use their *expectation values* as macrovariables to identify macrostates and compute an entropy function by maximizing the Gibbs-von Neumann entropy, given those expectation values.

   The wavepackets that we construct are located at discrete space and momentum points, denoted $\alpha \equiv (r, v)$, and localized on a scale of $\hbar$. We show that the average occupancy of these states denoted D_α, constitute a coarse-graining of the Wigner function on a scale of $\hbar$. Unlike the Wigner function, D_α is positive and is thus similar to the so-called Husimi function [31]. However, the Husimi function has the full information on the one-particle density matrix and so for non-interacting systems, it cannot be used for the construction of an entropy function. The function D_α incorporates coarse-graining required to demonstrate entropy growth in the quantum ideal gas. We note that the Wehrl entropy [32] uses the Husimi function and has been used to study irreversibility in interacting quantum systems [33,34,35].

   Our f-macrostate entropy, S_B^f, also increases with time and reaches a steady state saturation value. In this case, the entropy growth is oscillatory with a period given by $L/\Delta p$ where Δp is the momentum coarse-graining scale – this can be understood from semi-classical considerations. The change in entropy per particle satisfies the bound $\ln 2 \leq \Delta s_B^f \leq 2\ln 2$ for fermions and $0 \leq \Delta s_B^f \leq \ln 2$ for bosons. This can be understood from the momentum distribution in the final state.

3. Results obtained for the evolution of pure states were compared with those of corresponding thermal initial states and we showed evidence of their equivalence at larger system sizes. This demonstrates typicality in the dynamical evolution. Bosons showed

larger finite size effects at low temperatures because of the fact that a relatively smaller number of single-particle levels are occupied and number fluctuations are larger.

4. From the single-particle spectrum on the circle, it is clear that the system has an exact recurrence at a time $\tau_{rec} = L^2/\pi$ (in units of $m = \hbar = 1$). However for both our macrovariables, relaxation to the steady state occurs on a time scale $\tau_{eq} \sim L$ and so, in the thermodynamic limit $L, N \to \infty$ with L/N constant, there is a clear separation between the relaxation and recurrence time-scales. This kind of recurrence is expected whenever the single-particle spectrum is given in terms of integers and would be observed in quantum particles in harmonic traps but would not be present in generic anharmonic potentials (see for e.g [36]).

As expected, our system does not reach a Gibbs equilibrium state. The final effective temperature and chemical potential corresponding to the final particle and energy density do not determine the true single-particle momentum distribution, which is not able to attain thermal equilibrium for the quantum ideal gas. This is different from the classical gas, where an initial Maxwell velocity distribution would continue to be the correct equilibrium velocity distribution for the expanded gas. In the quantum gas, it would be necessary to include interactions to allow the momentum distribution to relax to thermal equilibrium; this does not happen for the ideal quantum gas. A recent study considered Boltzmann's entropy growth in a classical interacting gas and interesting differences with the non-interacting case were noted [37]. The effect of interactions in the quantum case would be interesting to explore, however, this would then become a highly-entangled many-body system and thus very challenging to treat accurately.

8 Acknowledgements

A Marginals of the wavepacket density

Here we establish the fact mentioned in Sec. (5.2) that the marginals of the wave-packet density, D_α, after integrating either over momentum or space, correspond respectively to the coarse-grained particle density

and momentum density. Let us consider the momentum marginal first i.e. sum over r

$$
\begin{aligned}
D_v(v,t) = \sum_r D(r,v,t) &= \sum_{r,m,n} \langle r,v|m\rangle \tilde{\rho}_1(p_m,p_n,t)\langle n|r,v\rangle \\
&= \frac{1}{K}\sum_{r=1}^{K}\sum_{m,n\in\mathscr{R}_v} e^{2\pi i(m-n)r/K}\tilde{\rho}_1(p_m,p_n,t) \\
&= \sum_{n\in\mathscr{R}_v}\tilde{\rho}_1(p_n,p_n,0).
\end{aligned}
\tag{64}
$$

Let us now consider the r-marginal i.e. sum over v

$$
D_r(r,t) = \sum_v D(r,v,t) = \int \frac{dx\,dx'}{LK}\sum_v\sum_{m,n\in\mathscr{R}_v} Q_{mn}(x,x',t),
\tag{65}
$$

$$
Q_{mn}(x,x',t) = e^{2\pi i(-mx+nx')/L}e^{i(m-n)2\pi r/K}\rho_1(x,x',t).
\tag{66}
$$

Note that $m,n\in\mathscr{R}_v$ which is given by

$$
\mathscr{R}_v = \left\{v - \frac{K-1}{2}, \ldots, v + \frac{K-1}{2}\right\}.
\tag{67}
$$

We substitute $m = v + \tilde{m}$ and $n = v + \tilde{n}$ to get rid of the v dependence in the sums over m and n. We thus get

$$
D_r(r,t) = \int \frac{dx\,dx'}{LK}\sum_v\sum_{\tilde{m},\tilde{n}\in\mathscr{R}_0} e^{2\pi iv(x'-x)/L}Q_{\tilde{m}\tilde{n}}(x,x',t).
\tag{68}
$$

Now since v takes values ϑK where ϑ is an integer that runs from $-\infty$ to $+\infty$, the sum over v can be done and gives

$$
\begin{aligned}
D_r(r,t) &= \int \frac{dx\,dx'}{K^2}\sum_{\tilde{m},\tilde{n}\in\mathscr{R}_0}\delta(x-x')Q_{\tilde{m}\tilde{n}}(x,x',t) \\
&= \int_0^L \frac{dx}{K^2}\left|\sum_{\tilde{n}=-(K-1)/2}^{(K-1)/2}\exp\left[2\pi i\tilde{n}\left(\frac{x}{L} - \frac{r}{K}\right)\right]\right|^2 \rho_1(x,x,t) \\
&= \int_0^L dx\, h_K\left(\frac{x}{L} - \frac{r}{K}\right) n(x,t),
\end{aligned}
\tag{69}
$$

where $n(x,t)$ is the particle density and $h_K(x) = \dfrac{1}{K^2}\left(\dfrac{\sin\pi Kz}{\sin\pi z}\right)^2$.

B Dependence on K

Here we briefly discuss the dependence of our results on the coarse-graining parameter K.

Fermions: In Fig. (13), we plot the saturation value $s_B^f(\infty)$ for different K and for the low and intermediate temperatures. We observe that as long as $K \ll L$, the saturation value does not vary strongly with K. Also, the variation becomes smaller with increasing temperature.

Bosons: The strong dependence on K can be understood from Fig. (14) which shows the variation of the saturation value of the f-macrostate entropy per particle with K. Here, we can clearly see that the variation is stronger for bosons as compared to fermions. As a result, the K values used in our numerical study are not small enough compared to the system size L for bosons, especially in the low-temperature case.
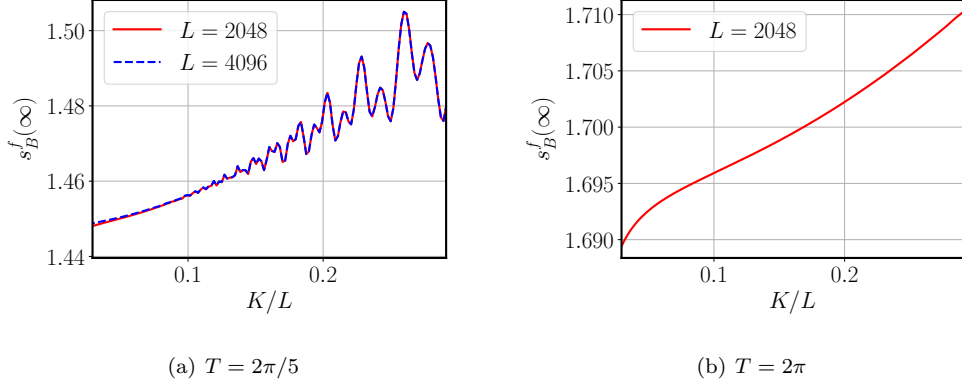
(a) $T = 2\pi/5$ (b) $T = 2\pi$

Fig. 13 Fermions: The late time value of the f-macrostate entropy per particle, $s_B^f(\infty)$ as a function of the coarse-graining scale K for the low and intermediate temperatures. It seems that we require $K/L \ll 1$ for the final value to not vary strongly with K. The variation also goes down with increasing temperature.
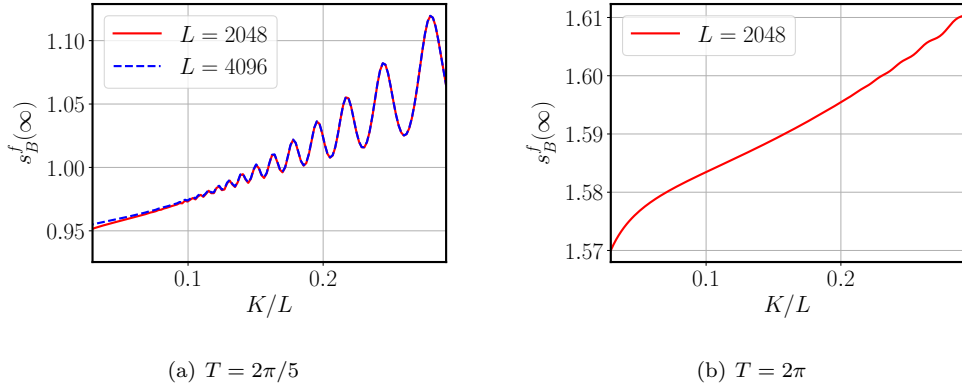

(a) $T = 2\pi/5$ (b) $T = 2\pi$

Fig. 14 Bosons: The late time value of the f-macrostate entropy per particle, $s_B^f(\infty)$ as a function of the coarse-graining scale K for the low and intermediate temperatures. It seems that we require $K/L \ll 1$ for the final value to not vary strongly with K. Also note that the variation with K is stronger for bosons as compared to fermions, so a relatively smaller K/L may be required for bosons. Here also, the variation goes down with increasing temperature.

C Glossary

– f, U: denote the two macrovariables studied in this work.
– S_B^f, S_B^U: the Boltzmann entropies corresponding to the two macrovariables.
– s_B^f, s_B^U: Boltzmann entropies per particle.
– X: Phase space point.
– $|\Phi\rangle$: Pure state wavefunction.
– N, E, L: The total number of particles, the total energy, and the system size (Circle perimeter) respectively.
– T, β, μ: The temperature, the inverse temperature, and the chemical potential respectively.
– a: Fraction of the circle occupied by the gas at time $t = 0$. In most cases $a = 1/2$.
– m: Mass of the particles.

- $\mathscr{H}$: Hilbert space.
- $\mathscr{H}_E$: Subspace of the full Hilbert space corresponding to the energy E.
- $\hat{M}_k$: Generic self-adjoint operators.
- $\nu, \mathscr{H}_\nu$: Generic macrostate and the corresponding macro-space.
- $|\mathscr{H}_\nu|$: Denotes the dimension of the $\mathscr{H}_\nu$ macro-space.
- $\hat{P}_\nu$: Projection operator onto the $\mathscr{H}_\nu$ macro-space.
- S_ν: Boltzmann entropy corresponding to the ν macrostate.
- $\mathscr{H}_{eq}$: Equilibrium macro-space.
- $\hat{\rho}_{\mathrm{GC}}, Z_{\mathrm{GC}}$: Generalized canonical density operator and the corresponding partition function.
- λ_k: Lagrange multipliers (for satisfying the constraints) in the expression for $\hat{\rho}_{\mathrm{GC}}$.
- S_{GvN}: The Gibbs-von Neumann entropy of the system
- δ, A: Denote the size and number respectively of the coarse-grained cells in the U-macrostate.
- ℓ: Labels the coarse-grained cells in the U-macrostate.
- $\hat{N}_\ell, \hat{P}_\ell, \hat{E}_\ell$: Denote the particle number, the momentum, and the energy operators respectively corresponding to the ℓth cell in the U-macrostate.
- K: Denotes the coarse-graining scale in the f-macrostate.
- $|\psi_\alpha\rangle \equiv |r, v\rangle$: The wavepacket basis state localized in position around $x = rL/K$ and in momentum around $p = 2\pi\hbar v/L$.
- $\hat{n}_\alpha, D_\alpha(t) \equiv D(r, v, t)$: Denote the occupation number operator and the average occupancy (wavepacket density) respectively of the wavepacket basis state $|\psi_\alpha\rangle$.
- $|\chi_s\rangle, e_s, n_s$: Denote the box energy eigenfunction, eigenvalue, and occupancy of the sth level respectively.
- $|\varphi_n\rangle, p_n, \epsilon_n$: Denote the circle energy eigenfunction, momentum, and energy eigenvalue of the nth level respectively.
- $\hat{\Psi}_x, \hat{b}_n$: Denote the annihilation operator in the position and in momentum space respectively.
- $\hat{\rho}_N$: The N-particle density operator.
- $\hat{\rho}_1, \rho_1(x, x'), \tilde{\rho}_1(p_m, p_n)$: The single-particle density operator and its matrix elements in the position and momentum space respectively.
- V: Transformation matrix from the box to the circle basis.
- $f(e_s, \beta, \mu)$: Denotes the Fermi/Bose function.
- $\hat{\rho}_1^P, \hat{\rho}_1^M$: Denote the single-particle density operator corresponding to the pure and mixed state initial conditions respectively.
- $P(\{n_s\})$: Denotes the grand canonical probability distribution of the configuration $\{n_s\}$.
- $w(x, p, t)$: The Wigner function on the real line.
- q_n: Denotes the half-integer momenta on the circle.
- $w(x, q_n, t)$: The Wigner function on the circle.
- $\hat{N}, \hat{P}, \hat{E}$: Denote the total particle number, the total momentum, and the total energy operators respectively.
- $\hat{n}(x, t), \hat{p}(x, t), \hat{e}(x, t)$: Denote the local particle, momentum, and energy density operators respectively.
- $n(x, t), p(x, t), e(x, t)$: Denote the expectation values of the local particle, momentum, and energy density operators respectively.
- $\mathscr{R}_v$: The set of K integers centered around v.
- $v_\pm$: The two end points of the set $\mathscr{R}_v$.
- $G_K(q, x)$: The localized kernel that, when integrated over the Wigner function, yields the wavepacket density.
- $D_r(r, t), D_v(v, t)$: The respective marginals of $D(r, v, t)$.
- $h_K(x)$: The localized kernel that, when integrated with the particle density $n(x, t)$, yields the coarse-grained marginal $D_r(r, t)$.
- $\hat{\rho}_N^\star$: Maximal N-particle density operator subject to the wavepacket density constraints.
- λ_α: Lagrange multipliers (for satisfying the constraints) in the expression for $\hat{\rho}_N^\star$.
- $\Delta s_B^f, \Delta s_B^U$: The final change in the entropies of f and U macrostates respectively.
- ρ: Particle density N/L.
- λ_{th}: The thermal De-Broglie wavelength.
- τ_p: The period of oscillations of the particle density.
- v_{f}: Fermi velocity.
- τ: The period of oscillations of the Boltzmann entropy S_B^f.
- τ_{rec}: The recurrence period.

References

1. L. Boltzmann, "On Zermelo's paper "On the mechanical explanation of irreversible processes"," *Annalen der Physik*, vol. 60, pp. 392–398, 1897.
2. R. Feynman, *The Character of Physical Law, with new foreword.* MIT press, 2017.
3. O. E. Lanford, "On a derivation of the boltzmann equation," *Astérisque*, vol. 40, no. 117, pp. 0353–70020, 1976.
4. R. Penrose and N. D. Mermin, "The emperor's new mind: Concerning computers, minds, and the laws of physics," 1990.
5. B. Greene, *The fabric of the cosmos: Space, time, and the texture of reality.* Knopf, 2004.
6. J. L. Lebowitz, "Macroscopic laws, microscopic dynamics, time's arrow and boltzmann's entropy," *Physica A: Statistical Mechanics and its Applications*, vol. 194, no. 1-4, pp. 1–27, 1993.
7. J. L. Lebowitz, "Boltzmann's entropy and time's arrow," *Physics Today*, vol. 46, no. 9, p. 32, 1993.
8. S. Goldstein and J. L. Lebowitz, "On the (Boltzmann) entropy of non-equilibrium systems," *Physica D*, vol. 193, no. 1, p. 53, 2004.
9. R. Griffiths, "Statistical irreversibility: classical and quantum.," *Physical origins of time asymmetry*, pp. 147–159, 1994.
10. S. Goldstein, D. A. Huse, J. L. Lebowitz, and R. Tumulka, "Macroscopic and microscopic thermal equilibrium," *Annalen der Physik*, vol. 529, no. 7, p. 1600301, 2017.
11. H. Tasaki, "Typicality of thermal equilibrium and thermalization in isolated macroscopic quantum systems," *Journal of Statistical Physics*, vol. 163, no. 5, pp. 937–997, 2016.
12. T. Mori, T. N. Ikeda, E. Kaminishi, and M. Ueda, "Thermalization and prethermalization in isolated quantum systems: a theoretical overview," *Journal of Physics B: Atomic, Molecular and Optical Physics*, vol. 51, no. 11, p. 112001, 2018.
13. W. De Roeck, C. Maes, and K. Netočnỳ, "Quantum macrostates, equivalence of ensembles, and an h-theorem," *Journal of mathematical physics*, vol. 47, no. 7, p. 073303, 2006.
14. H. B. Callen, "Thermodynamics and an introduction to thermostatistics," 1998.
15. S. Chakraborti, A. Dhar, S. Goldstein, A. Kundu, and J. L. Lebowitz, "Entropy growth during free expansion of an ideal gas," 2021.
16. D. S. Dean, P. Le Doussal, S. N. Majumdar, and G. Schehr, "Wigner function of noninteracting trapped fermions," *Phys. Rev. A*, vol. 97, p. 063614, Jun 2018.
17. M. Kulkarni, G. Mandal, and T. Morita, "Quantum quench and thermalization of one-dimensional fermi gas via phase-space hydrodynamics," *Phys. Rev. A*, vol. 98, p. 043610, Oct 2018.
18. V. Eisler and Z. Rácz, "Full counting statistics in a propagating quantum front and random matrix spectra," *Physical review letters*, vol. 110, no. 6, p. 060602, 2013.
19. S. Scopa, A. Krajenbrink, P. Calabrese, and J. Dubail, "Exact entanglement growth of a one-dimensional hard-core quantum gas during a free expansion," *Journal of Physics A: Mathematical and Theoretical*, vol. 54, no. 40, p. 404002, 2021.
20. L. F. Santos, A. Polkovnikov, and M. Rigol, "Entropy of isolated quantum systems after a quench," *Phys. Rev. Lett.*, vol. 107, p. 040601, Jul 2011.
21. D. Šafránek, J. M. Deutsch, and A. Aguirre, "Quantum coarse-grained entropy and thermodynamics," *Physical Review A*, vol. 99, no. 1, p. 010101, 2019.
22. D. Šafránek, J. Deutsch, and A. Aguirre, "Quantum coarse-grained entropy and thermalization in closed systems," *Physical Review A*, vol. 99, no. 1, p. 012103, 2019.
23. E. Solano-Carrillo and A. Millis, "Theory of entropy production in quantum many-body systems," *Physical Review B*, vol. 93, no. 22, p. 224305, 2016.
24. E. Fick, G. Sauermann, and W. D. Brewer, *The quantum statistics of dynamic processes*, vol. 86. Springer, 1990.
25. E. Wigner, "On the quantum correction for thermodynamic equilibrium," *Phys. Rev.*, vol. 40, pp. 749–759, Jun 1932.
26. M. Hillery, R. F. O'Connell, M. O. Scully, and E. P. Wigner, "Distribution functions in physics: Fundamentals," *Physics reports*, vol. 106, no. 3, pp. 121–167, 1984.
27. N. Mukunda, "Algebraic aspects of the wigner distribution in quantum mechanics," *Pramana*, vol. 11, no. 1, pp. 1–15, 1978.
28. N. Mukunda, "Wigner distribution for angle coordinates in quantum mechanics," *American Journal of Physics*, vol. 47, no. 2, pp. 182–187, 1979.
29. M. V. Berry, "Semi-classical mechanics in phase space: a study of wigner's function," *Philosophical Transactions of the Royal Society of London. Series A, Mathematical and Physical Sciences*, vol. 287, no. 1343, pp. 237–271, 1977.

30. A. Dhar , *to be published*.
31. K. Husimi, "Some formal properties of the density matrix," *Proceedings of the Physico-Mathematical Society of Japan. 3rd Series*, vol. 22, no. 4, pp. 264–314, 1940.
32. A. Wehrl, "On the relation between classical and quantum-mechanical entropy," *Reports on Mathematical Physics*, vol. 16, no. 3, pp. 353–358, 1979.
33. H. Tsukiji, H. Iida, T. Kunihiro, A. Ohnishi, and T. T. Takahashi, "Entropy production from chaoticity in yang-mills field theory with use of the husimi function," *Physical Review D*, vol. 94, no. 9, p. 091502, 2016.
34. T. Kunihiro, B. Müller, A. Ohnishi, and A. Schäfer, "Towards a theory of entropy production in the little and big bang," *Progress of theoretical physics*, vol. 121, no. 3, pp. 555–575, 2009.
35. B. O. Goes, G. T. Landi, E. Solano, M. Sanz, and L. Céleri, "Wehrl entropy production rate across a dynamical quantum phase transition," *Physical Review Research*, vol. 2, no. 3, p. 033419, 2020.
36. D. S. Dean, P. Le Doussal, S. N. Majumdar, and G. Schehr, "Nonequilibrium dynamics of noninteracting fermions in a trap," *EPL (Europhysics Letters)*, vol. 126, no. 2, p. 20006, 2019.
37. S. Chakraborti, A. Dhar, and A. Kundu, "Boltzmann's entropy during free expansion of an interacting gas," *Journal of Statistical Physics*, vol. 190, no. 4, p. 74, 2023.